Physica C 198 (1992) 309–317
North-Holland

PHYSICA C

Structural properties of stage-1 iodine-intercalated superconducting $I(Bi_{0.915}, Pb_{0.085})_2(Sr_{0.93}, Pb_{0.07})_2(Ca_{0.965}, Pb_{0.035})_2Cu_3O_x$

N. Kijima
Research Center, Mitsubishi Kasei Corporation, 1000 Kamoshida-cho, Midori-ku, Yokohama 227, Japan

R. Gronsky
Department of Materials Science & Mineral Engineering, University of California, and National Center for Electron Microscopy, Materials Sciences Division, Lawrence Berkeley Laboratory, Berkeley, CA 94720, USA

X.-D. Xiang, W.A. Vareka, J. Hou, A. Zettl, J.L. Corkill and Marvin L. Cohen
Department of Physics, University of California, and Materials Sciences Division, Lawrence Berkeley Laboratory, Berkeley, CA 94720, USA

Received 24 April 1992

The crystal structure of stage-1 iodine-intercalated superconducting $I(Bi_{0.915}, Pb_{0.085})_2(Sr_{0.93}, Pb_{0.07})_2(Ca_{0.965}, Pb_{0.035})_2Cu_3O_x$ has been determined by transmission electron microscopy to belong to the space group Pma2 with lattice parameters $a=5.4$ Å, $b=5.4$ Å and $c=22.0$ Å. Iodine atoms intercalated as monolayers between every Bi–O bilayer alter the atomic stacking across Bi–O layers from the staggered configuration characteristic of superconducting $(Bi_{0.915}, Pb_{0.085})_2(Sr_{0.93}, Pb_{0.07})_2(Ca_{0.965}, Pb_{0.035})_2Cu_3O_x$ to a vertically aligned configuration in $I(Bi_{0.915}, Pb_{0.085})_2(Sr_{0.93}, Pb_{0.07})_2(Ca_{0.965}, Pb_{0.035})_2Cu_3O_x$. Iodine bilayers have also been observed to form between Bi–O layers, yielding a new series of stage-n iodine-intercalated compounds.

1. Introduction

Recently, a number of stage-1 iodine-intercalated $Bi_2Sr_2Ca_{n-1}Cu_nO_x$ ($n=1, 2, 3$) superconductors and a stage-2 iodine-intercalated $IBi_4Sr_4Ca_2Cu_4O_x$ superconductor were discovered, and the superconducting response of these materials was related to the amount of lattice expansion induced along the c-axis owing to intercalation [1–5]. Beginning with a host superconductor with composition $Bi_2Sr_2CaCu_2O_x$, iodine was interacalated between every Bi–O bilayer in the temperature range of 150 to 200°C for aging times between 10 and 15 days. At higher temperature (300°C), iodine intercalation only occurred between every other Bi–O bilayer of the host superconductor, after the same aging times (10 to 15 days). It was found from the temperature dependence of the AC and DC magnetic susceptibilities that the stage-1 iodine-intercalated compound $IBi_2Sr_2CaCu_2O_x$ behaves as a bulk superconductor, but with a superconducting transition temperature (T_c) 10 K lower than the host material from which it was fabricated. The state-2 iodine-intercalated superconducting compound $IBi_4Sr_4Ca_2Cu_4O_x$ exhibited a T_c that was only 5 K lower than the host superconductor $Bi_2Sr_2CaCu_2O_x$. The crystal structures of both the stage-1 iodine-intercalated $IBi_2Sr_2CaCu_2O_x$ and stage-2 iodine-intercalated $IBi_4Sr_4Ca_2Cu_4O_x$ were determined by X-ray diffraction analysis [2] and transmission electron microscopy [3–5]. These studies showed that iodine atoms occupied specific, epitaxial sites between the Bi–O bilayers and caused a corresponding expansion along the c-axis of 3.6 Å for each Bi–O bilayer. The intercalated iodine atoms also altered the atomic stacking across Bi–O layers from the staggered configuration characteristic of superconducting $Bi_2Sr_2CaCu_2O_x$ to a registered configuration in $IBi_2Sr_2CaCu_2O_x$ and $IBi_4Sr_4Ca_2Cu_4O_x$. In the crystal structure of the stage-2 iodine-intercalated superconductor, however, the

c-axis dimension was found to be 7.1 Å shorter than 4 times the c-axis dimension of the stage-1 iodine-intercalated superconductor. It was also conclude from the atomic spacings apparent in the high-resolution transmission electron microscope images of $IBi_2Sr_2CaCu_2O_x$ and $IBi_4Sr_4Ca_2Cu_4O_x$ that the iodine layers bond to their neighboring Bi–O layers by van der Waals interactions.

Many stacking faults were observed in those crystals which predominantly contain the stage-2 compound [5,6], and these materials also exhibited periodically dispersed stage-3 and higher-stage intercalated phases. The crystal structure of stage-3 iodine-intercalated superconducting $IBi_6Sr_6Ca_3Cu_6O_x$ was also determined by transmission electron microscopy [6]. Iodine atoms intercalated between every three Bi–O bilayers expand the distance between the Bi–O layers by 3.6 Å and alter the atomic stacking across Bi–O layers from the staggered configuration characteristic of the host superconducting $Bi_2Sr_2CaCu_2O_x$ to an aligned configuration characteristic of the stage-1 iodine-intercalated superconducting $IBi_2Sr_2CaCu_2O_x$. Higher-stage intercalation appeared in the form of stacking faults in these materials with both stage-2 and stage-3 phases. The space groups and c-axis dimensions of the higher-stage phases $IBi_{2n}Sr_{2n}Ca_nCu_{2n}O_x$ were deduced to be Pma2 with $c=3.6+15.3n$ Å when stage number n is odd, and Bbmb with $c=2(3.6+15.3n)$ Å when n is even.

The present study is an extension of this research, employing a Pb-doped compound to examine the effect of intercalation on its structure. Beginning with host superconducting Pb-doped $Bi_2Sr_2Ca_2Cu_3O_x$ (ideal compostion), we synthesized an iodine-intercalated Pb-doped $Bi_2Sr_2Ca_2Cu_3O_x$ and determined the details of its crystal structure using techniques of high-resolution transmission electron microscopy.

2. Experimental

A host specimen was prepared by a sol–gel process using citric salts. The starting materials were high-purity powders of PbO, Bi_2O_3, $SrCO_3$, $CaCO_3$ and CuO. These powders were dissolved in nitric acid, mixed with citric acid and ethylene glycol, and then heated to obtain a blue gel. The gel was subsequently calcined at 800°C for 30 min, ground, pressed into a pellet and fired at 850°C for 18 days in air. The bulk crystal structure and chemical composition of the host specimen were obtained by Rietveld analyses of powder X-ray diffraction data and energy X-ray spectroscopy, the procedures for which are described in a former paper [7].

The sintered host specimen was thinned, dimpled, and ion-milled to electron transparency. Ion milling was carried out at 77 K using argon ions accelerated at 3 kV and an incidence angle of 12 degrees. A polycrystalline specimen of the iodine-intercalated superconductor $I(Bi_{0.915}, Pb_{0.085})_2(Sr_{0.93}, Pb_{0.07})_2(Ca_{0.965}, Pb_{0.035})_2Cu_3O_x$ (which will be simplified to $IPb_yBi_2Sr_2Ca_2Cu_3O_x$) was next prepared by encapsulating iodine and the ion-milled specimen of $(Bi_{0.915}, Pb_{0.085})_2(Sr_{0.93}, Pb_{0.07})_2(Ca_{0.965}, Pb_{0.035})_2Cu_3O_x$ (simplified to $Pb_yBi_2Sr_2Ca_2Cu_3O_x$) in a Pyrex tube under a vacuum of $<10^{-3}$ torr. Iodine interaction was carried out at 150°C for 2 h in a uniform-temperature furnace.

In order to clean the surface of the specimen, ion milling was again used briefly after intercalation. Transmission electron microscopy was performed in the Berkeley JEM ARM-1000 operating at 800 kV. Images were Fourier filtered, using the image processing program SEMPER [8], and compared with images simulated by the code NCEMSS [9] at the National Center for Electron Microscopy.

3. Results and Discussion

Figure 1 depicts selected area electron diffraction patterns of the iodine-intercalated Pb-doped compound in four different zone axes, with fig. 1(b) showing the presence of a 90° twin. Electron diffractions from both the a^*–c^* and b^*–c^* planes are simultaneously observed in fig. 1(b). Lattice parameters determined from direct measurements of these patterns are $a=5.4$ Å, $b=5.4$ Å and $c=22.0$ Å. The a and b axial lengths are identical to those of the host material, while the c parameter is 3.5 Å longer than half of the c parameter (37.05 Å) in the host material. The corresponding reciprocal lattice is drawn in fig. 2, showing both all primary and satellite reflections observed in figs. 1(a)–(d). Primary reflections with indices $h0l(h=2n+1)$ show extinctions,

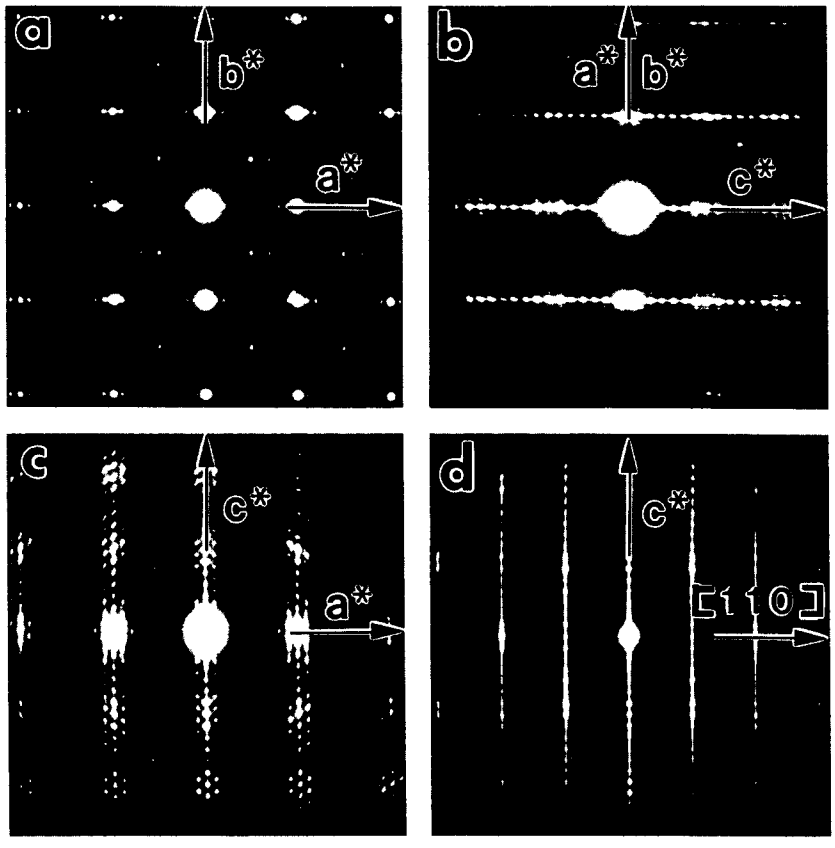

Fig. 1. Selected area electron diffraction patterns of the stage-1 iodine-intercalated superconductor $I(Bi_{0.915}, Pb_{0.085})_2(Sr_{0.93}, Pb_{0.07})_2(Ca_{0.965}, Pb_{0.035})_2Cu_3O_x$. (a) a^*–b^* plane, (b) b^*–c^* plane and a^*–c^* plane from a 90° twinned crystal, (c) a^*–c^* plane, (d) [110]–c^* plane.

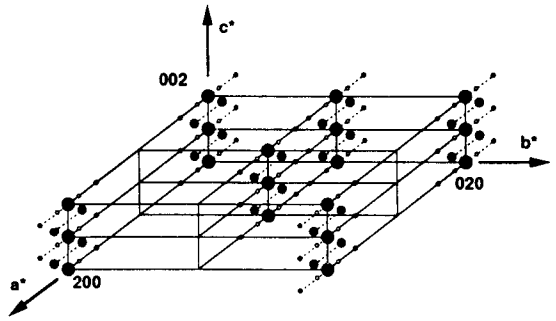

Fig. 2. Reciprocal lattice showing both primary reflections and satellite reflections based upon the selected area electron diffraction patterns in fig. 1.

indicating that the candidate space groups for this crystal structure include Pma2, Pmam (equivalent to Pmma) and $P2_1am$ (equivalent to $Pmc2_1$). As in the stage-1 iodine-intercalated superconducting $IBi_2Sr_2CaCu_2O_x$, no equivalent Bi atoms are observed in high-resolution micrographs along the a-axis at positions defined by the symmetry operation 2_1. Therefore, the space group of the stage-1 iodine-intercaland superconductor $IPb_yBi_2Sr_2Ca_2Cu_3O_x$ is concluded to be Pma2, which is the same as the stage-n iodine-intercalated compounds $IBi_{2n}Sr_{2n}Ca_nCu_{2n}O_x$ when n is odd.

There are two types of satellite reflections in the a^*–c^* reciprocal plane; one is marked A and the other is marked B in fig. 3. The A satellites are related to the primary reflections by a vector with an irrational component along the a^*-axis and a rational component along the c^*-axis. The a-axis component has a corresponding wavelength of 27 Å, while the c-axis component has a wavelength which is twice the c lattice parameter. Assigning four indices H, K, L, and m to the satellites in accordance with the procedure described by de Wolff et al. [10], it is found that the allowed satellites have indices $HKLm(L+m=2n)$

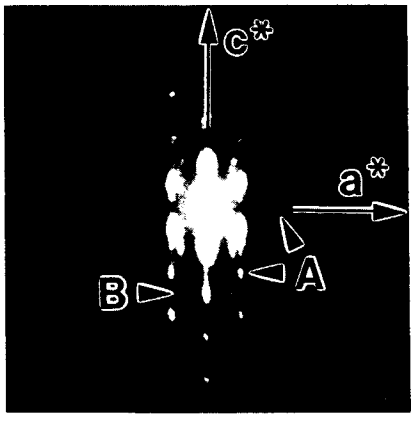

Fig. 3. Enlargement of the selected area electron diffraction pattern shown in fig. 1(c). There are two types of satellite reflection marked A and B within the a^*–c^* plane.

and $H0Lm(H=2n)$ where $H=h$, $K=k$, $L=2l+m$. This corresponds to the superspace group $C^{Pma2}_{1\,1\,1}$, or equivalently, $B^{Pc2m}_{1\,1\,1}$. The B satellites are related to primary reflections by a vector with only an irrational component along the a^*-axis, and a corresponding wavelength of 35 Å. It is found that the allowed satellites have indices $H0Lm(H=2n)$ where $H=h$, $K=k$, $L=l$. This corresponds to the superspace group $P^{Pma2}_{1\,1\,1}$ or, equivalently, $P^{P2cm}_{1\,1\,1}$. Both types of satellite reflections are also observed in the host material [11–13]. It follows that intercalated iodine has little or no effect on the modulated structure of these materials, in spite of its large atomic radius. It is therefore most probable that the nature of the chemical bonding between the iodine layer and the Bi–O bilayers is weak enough to have no effect on the bonds formed within the adjacent Bi–O layers, as in the stage-1 iodine-intercalated superconducting $IBi_2Sr_2CaCu_2O_x$.

Figure 4 shows a phase-contrast high-resolution transmission electron micrograph with the incident electron beam along the a-axis. Atomic resolution has been achieved in this image which shows that iodine atoms (marked by arrows) intercalate as monolayers between every Bi(Pb)–O bilayer. This structure resembles the stage-1 iodine-intercalated superconductor $IBi_2Sr_2CaCu_2O_x$. Most of the crystals imaged in this way exhibit the same crystal structure; however, some has additional stacking faults as describe below.

Figure 5 shows an original high-resolution transmission electron micrograph (a), the corresponding processed image (b) and the simulated image (c) with the electron beam incident on the 3 nm thick

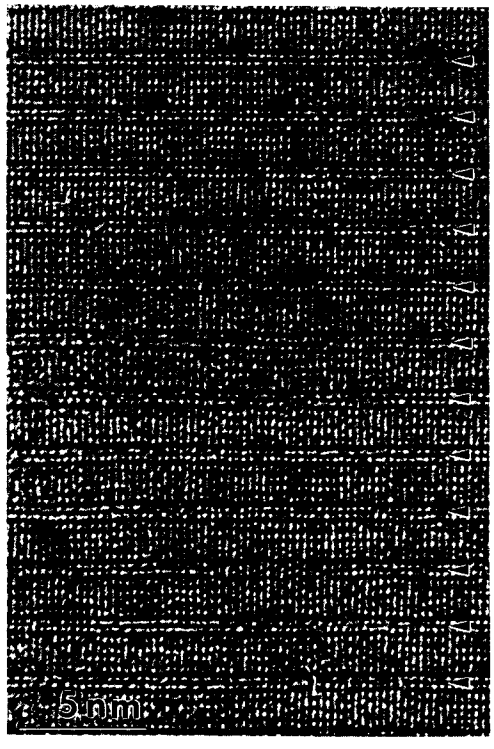

Fig. 4. Phase contrast high-resolution transmission electron micrograph of the stage-1 iodine-intercalated superconductor $I(Bi_{0.915}, Pb_{0.085})_2(Sr_{0.93}, Pb_{0.07})_2(Ca_{0.965}, Pb_{0.035})_2Cu_3O_x$ with the incident electron beam along the a-axis.

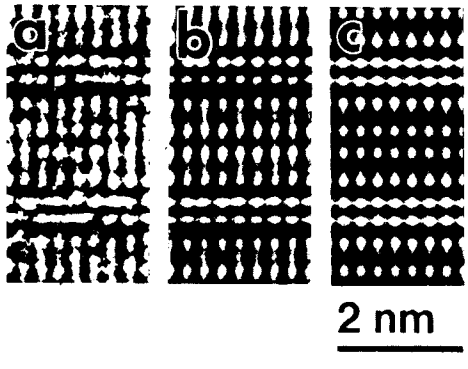

Fig. 5. Phase contrast high-resolution electron microscope image (a), corresponding processed image (b) and simulated image (c) of a 3 nm thick stage-1 iodine-intercalated superconducting $I(Bi_{0.915}, Pb_{0.085})_2(Sr_{0.93}, Pb_{0.07})_2(Ca_{0.965}, Pb_{0.035})_2CuO_x$ crystal, with an objective lens defocus −60 nm and the incident electron beam along the a-axis.

sample in a [100] orientation. Figure 6 shows a similar composite of the original high-resolution transmission electron micrograph (a), the corresponding processed image (b) and the simulated image (c), this time for a 6 nm thick sample and a [$\bar{1}$10] incident beam direction. Agreement in every case is acceptable, confirming the structural model used in the simulations. Table 1 summarizes all atomic positions within the intercalated crystal used for this study. In the image simulation, Pb concentrations at the Bi, Sr, and Ca sites were fixed to those values determined by the Rietveld analysis and cross-checked by energy dispersive X-ray spectroscopy.

Figure 7 shows the crystal structure of the stage-1 iodine-intercalated superconductor IPb_y-$Bi_2Sr_2Ca_2Cu_3O_x$, while figure 8 compares the structures of the stage-1 iodine-intercalated superconductors $IBi_2Sr_2CaCu_2O_x$ and $IPb_yBi_2Sr_2Ca_2Cu_3O_x$ with their pristine host superconductors $Bi_2Sr_2CaCu_2O_x$ and $Pb_yBi_2Sr_2Ca_2Cu_3O_x$. The stage-1 iodine-intercalated superconductors $IBi_2Sr_2CaCu_2O_x$ and $IPb_yBi_2Sr_2Ca_2Cu_3O_x$ have the same basic building blocks of Pb, Bi, Sr, Ca, Cu and oxygen as the host crystals $Bi_2Sr_2CaCu_2O_x$ and $Pb_yBi_2Sr_2Ca_2Cu_3O_x$. Following intercalation, iodine atoms are inserted between the Bi(Pb)–O bilayers, and the effect on the surrounding lattice is most visible in images viewed along a [$\bar{1}$10] incident beam direction. In the host crystals, the basic building blocks are staggered by half of the *b* axial length (fig. 8(a,c)), while in the stage-1 iodine-intercalated crystals, they are not staggered (fig. 8(b,d)).

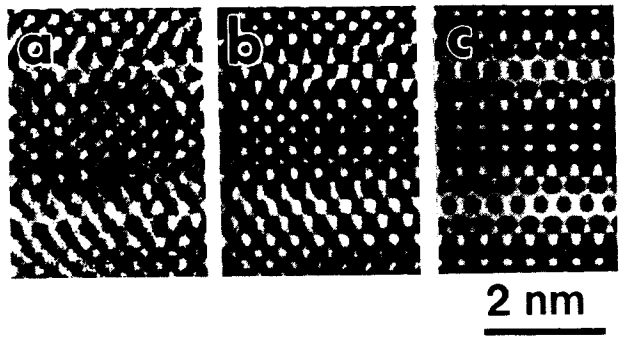

Fig. 6. Phase contrast high-resolution electron microscope image (a), corresponding processed image (b) and simulated image (c) of a 6 nm thick superconducting crystal, with an objective lens defocus −20 nm and the incident electron beam along the [$\bar{1}$10] direction.

Table 1
Atomic positions for the stage-1 iodine-intercalated superconductor $I(Bi_{0.915}, Pb_{0.085})_2(Sr_{0.93}, Pb_{0.07})_2(Ca_{0.965}, Pb_{0.035})_2Cu_3O_x$ used in image simulations

Atom	Site	x	y	z
I	2c	0.25	0.75	0.0
Bi(1)	2c	0.25	0.23	0.143
Bi(2)	2c	0.25	0.27	0.857
Sr(1)	2c	0.25	0.75	0.271
Sr(2)	2c	0.25	0.75	0.729
Ca(1)	2c	0.25	0.75	0.424
Ca(2)	2c	0.25	0.75	0.576
Cu(1)	2c	0.25	0.25	0.347
Cu(2)	2c	0.25	0.25	0.653
Cu(3)	2c	0.25	0.25	0.500
O(1)	2c	0.25	0.73	0.143
O(2)	2c	0.25	0.77	0.857
O(3)	2c	0.25	0.25	0.237
O(4)	2c	0.25	0.25	0.763
O(5)	2a	0.0	0.0	0.347
O(6)	2b	0.0	0.5	0.347
O(7)	2a	0.0	0.0	0.653
O(8)	2b	0.0	0.5	0.653
O(9)	2a	0.0	0.0	0.5
O(10)	2b	0.0	0.5	0.5

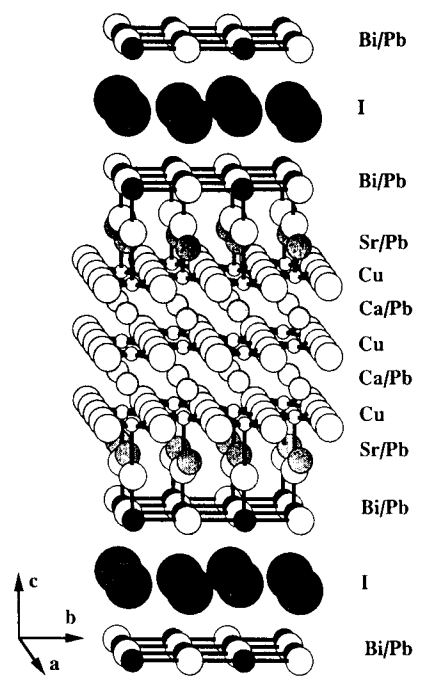

Fig. 7. Crystal structure of the stage-1 iodine-intercalated superconductor $I(Bi_{0.915}, Pb_{0.085})_2(Sr_{0.93}, Pb_{0.07})_2(Ca_{0.965}, Pb_{0.035})_2Cu_3O_x$.

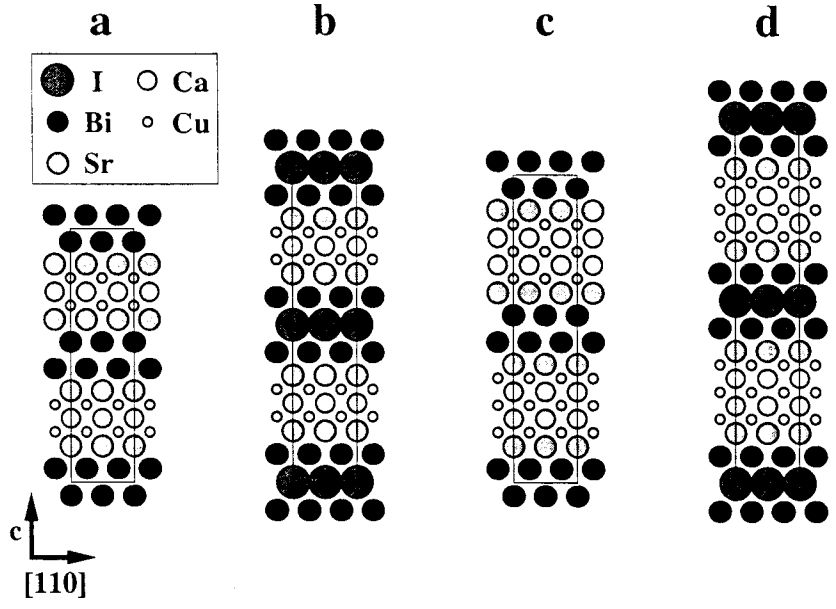

Fig. 8. Comparison of the crystal structures of the host superconductors ($Bi_2Sr_2CaCu_2O_x$ (a) and $(Bi_{0.915}, Pb_{0.085})_2(Sr_{0.93}, Pb_{0.07})_2(Ca_{0.965}, Pb_{0.035})_2Cu_3O_x$ (c)) and the stage-1 iodine-intercalated superconductors ($IBi_2Sr_2CaCu_2O_x$ (b) and $I(Bi_{0.915}, Pb_{0.085})_2(Sr_{0.93}, Pb_{0.07})_2(Ca_{0.965}, Pb_{0.035})_2Cu_3O_x$ (d)).

The actual location of iodine atoms in the Bi(Pb)–O bilayer of the stage-1 iodine-intercalated superconductor $IPb_yBi_2Sr_2Ca_2Cu_3O_x$ is the same as in the stage-1 iodine-intercalted superconductor $IBi_2Sr_2CaCu_2O_x$. In both cases, iodine atoms are surrounded by eight neighboring Bi(Pb) atoms. The relative positions of adjacent Bi(Pb) atoms in the stage-1 iodine-intercalated superconductors are the same as those of the Bi(Pb) atoms in those host crystals. It is therefore possible to model iodine intercalation as the simple substitution of I for Bi(Pb) atoms in one of the Bi(Pb)–O layers, resulting in the shift of the outwardly displaced Bi(Pb) atoms by half of the *b* axial length, so that the Bi(Pb) atoms in the upper (displaced) Bi(Pb)–O layer occupy lattice sites equivalent to Bi(Pb) atoms in the lower basic building block. This structural rearrangement results in a halving of the *c* axial length of $IPb_yBi_2Sr_2Ca_2Cu_3O_x$ relative to $Pb_yBi_2Sr_2Ca_2Cu_3O_x$.

Providing that there is no displacement of the oxygen atoms in the Bi(Pb)–O layer relative to the center of the adjacent four Bi(Pb) atoms, the interatomic distance between the iodine atoms and the oxygen atoms in the Bi(Pb)–O layer is 3.3 Å. This distance is approximately the same as the sum (3.55 Å) of the van der Waals radii of iodine and oxygen, which is a much better fit to the average interatomic distances between the iodine layer and the Bi–O bilayer than the summation of their covalent radii or iodine radii alone. Within the iodine layers, some covalent bonding is expected and the observed interatomic half-separation of the planar face-centered array is 1.9 Å, smaller than the iodine van der Waals radius of 2.15 Å.

Figure 9 is another high-resolution atomic resolution micrograph of the iodine-intercalated crystal, this time depicting a new iodine stacking sequence at the site of each arrow, highlighted by enlargement in fig. 10. The incident electron beam is again oriented along the $[\bar{1}10]$ direction in these images, which now clearly show two iodine layers between the Bi(Pb)–O layers of the original structure. There is also some long range order associated with the occurrence of the intercalated iodine bilayers, as labeled in fig. 9. At S1, every intercation site is filled by a double layer; at S2, every other intercalation site is a bilayer; and, at S3, every third intercalation site is a bilayer.

Figure 11 compares the Bi and I stacking sequences in the host material (a), the stage-1 iodine-intercalated structure (b), and the bilayer iodine intercalation structure (c). Note that, in the pristine

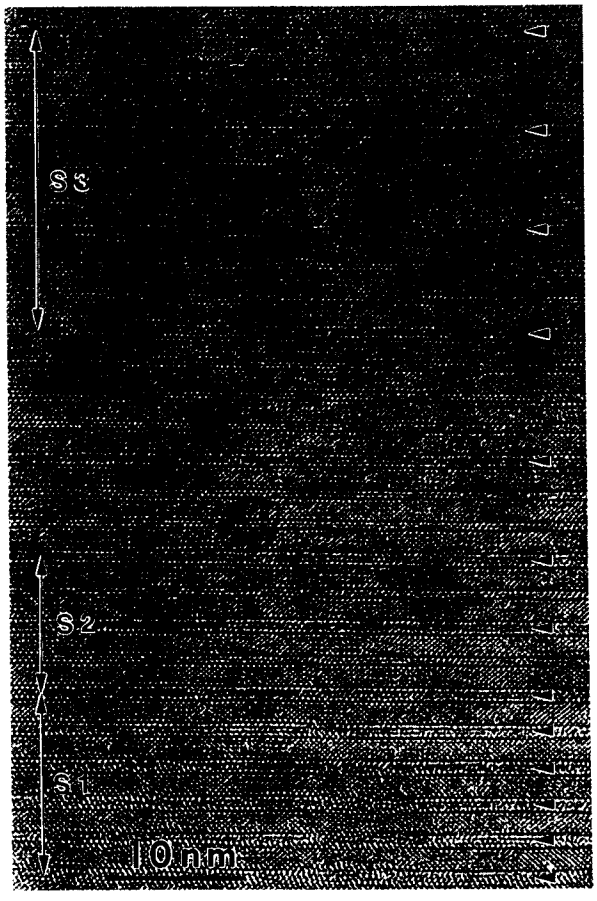

Fig. 9. High-resolution transmission electron micrograph of the iodine-intercalated crystal with a new, bilayer iodine stacking sequence. Double iodine layers are inserted between Bi–O bilayers at the iodine layers marked by arrows. This iodine bilayer stacking sequence is observed between every Bi–O bilayer in the region marked S1, every other Bi–O bilayer in the region marked S2 and every third Bi–O bilayer in the area marked S3.

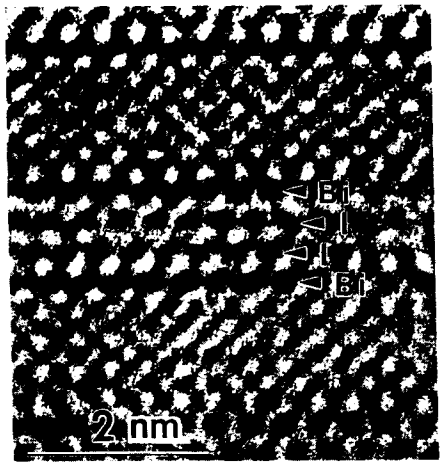

Fig. 10. Enlargement of the atomic resolution micrograph above, showing iodine bilayer intercalation. Two iodine layers marked I appear between Bi–O layers.

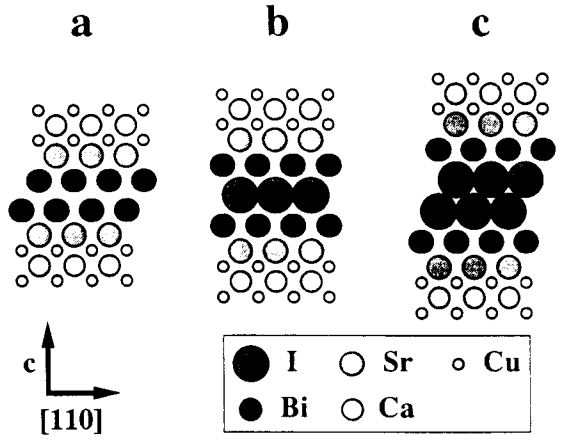

Fig. 11. Comparison of the Bi and I stacking sequences in the host material (a), stage-1 iodine-intercalated crystal (b) and the iodine bilayer intercalation (c).

host material, Bi atoms are staggered along the a-axis by half a unit cell. Iodine intercalation as a monolayer causes the Bi atoms to align vertically above one another but, as a bilayer, causes the original Bi atom stagger to be restored.

Direct measurements from the micrograph in fig. 9 yield the c lattice parameters of the intercalated polytypoids to be 51 Å at S1, 95 Å at S2 and 139 Å at S3. It is concluded from these measurements that monolayer iodine intercalation increases the distance between Bi–O layers by 3.5 Å (as observed in stage-1 iodine-intercalated superconducting crystal), while bilayer iodine intercalation increases this distance by 7.0 Å.

Ignoring differences caused by Pb substitution, for simplicity, it is probable that the ideal chemical compositions of the crystals occurring within regions S1, S2 and S3 of fig. 9 are $I_2Bi_2Sr_2Ca_2Cu_3O_x$, $I_3Bi_4Sr_4Ca_4Cu_6O_x$ and $I_4Bi_6Sr_6Ca_6Cu_9O_x$, respectively. Generalizing, for iodine bilayer intercalation between every n Bi–O bilayers, the chemical composition of the crystal will be $I_{n+1}Bi_{2n}Sr_{2n}Ca_{2n}Cu_{3n}O_x$, and its c lattice parameter will be $c=7+44n$ Å. All such structures may be described as having the space group Bbmb, due to the staggering of Bi–O layers across bilayer iodine layers, which is the same space group as the host superconductor.

From our previous studies, we know that monolayer iodine intercalation into $Bi_2Sr_2CaCu_2O_x$, to

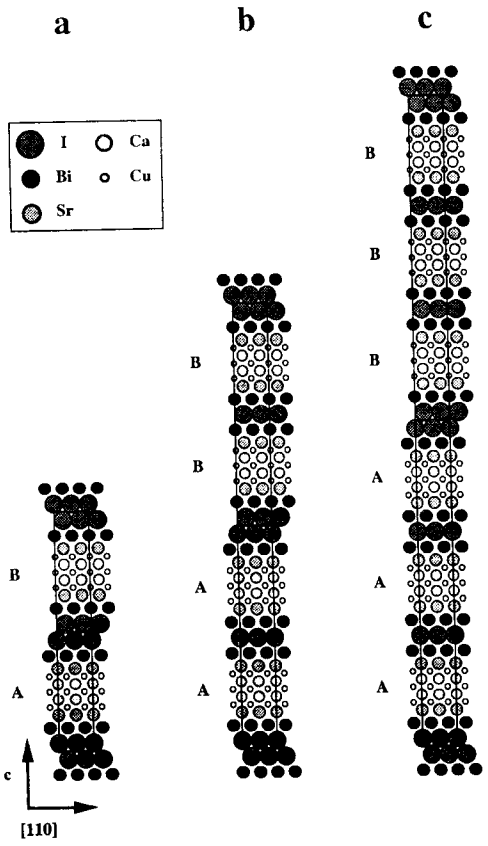

Fig. 12. Crystal structural models of the new series of the iodine-intercalated compounds which have two iodine layers between two Bi–O layers. Stage-1 iodine-intercalated compound $I_2Bi_2Sr_2Ca_2Cu_3O_x$ (a), stage-2 iodine-intercalated compound $I_3Bi_4Sr_4Ca_4Cu_6O_x$ (b) and stage-3 iodine-intercalated compound $I_4Bi_6Sr_6Ca_6Cu_9O_x$ (c).

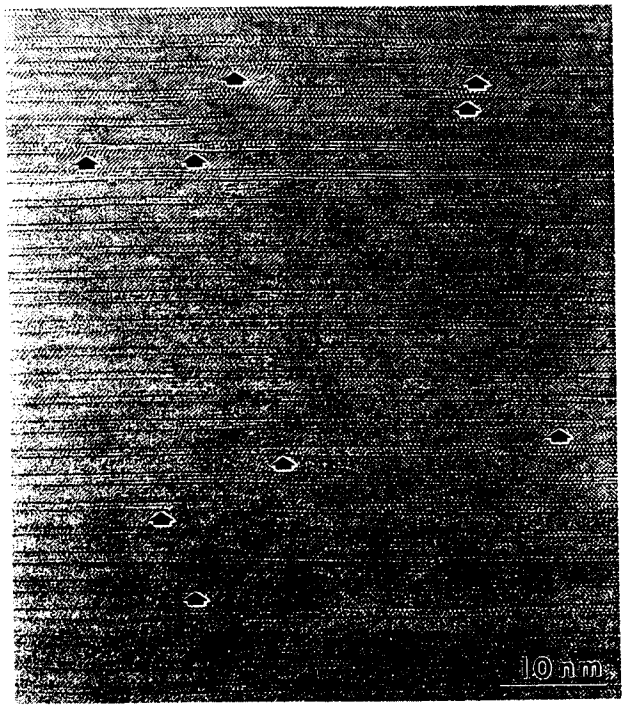

Fig. 13. Atomic resolution micrograph of same intercalated Pb-doped compound with incident electron beam along the [$\bar{1}$10] direction. Arrows show positions where the bifurcations from single iodine layers to double iodine layers between Bi–O bilayers occur.

form $IBi_{2n}Sr_{2n}Ca_nCu_{2n}O_x$, yields a structure with space group Pma2 and $c=3.6+15.3n$ Å when stage number n is odd, or space group Bbmb with $c=2(3.6+15.3n)$ Å when n is even [6]. These studies also demonstrated that higher stage structures result from higher intercalation temperatures [5]. In the present study, the stage-1 iodine-intercalated compound $IPb_yBi_2Sr_2Ca_2Cu_3O_x$ exhibits space groups Pma2 and c lattice parameter 22.0 Å when formed at 150°C. Higher-stage compounds $IPb_yBi_{2n}Sr_{2n}Ca_{2n}Cu_{3n}O_x$ ($n>1$) synthesized at higher temperatures have space group Pma2 and c lattice parameter given by $c=3.5+18.5n$ Å when stage number n is odd, or space group Bbmb with $c=2(3.5+18.5n)$ Å when n is even.

More importantly, the stage-1 iodine-intercalated superconductor $IPb_yBi_2Sr_2Ca_2Cu_3O_x$ is identified as the basic structure of a new series of iodine-intercalated compounds exhibiting iodine bilayers between Bi–O bilayers. By adding a second iodine layer between every Bi–O bilayer in the basic compound $IPb_yBi_2Sr_2Ca_2Cu_3O_x$, the stage-1 compound marked S1 in fig. 9 is synthesized. Similarly, the stage-2 and stage-3 compounds marked S2 and S3 are formed by intercalating iodine bilayers between every other or every third Bi–O bilayer in $IPb_yBi_2Sr_2Ca_2Cu_3O_x$, respectively. The crystal structures of all three polytypoids are compared in fig. 12. When a second iodine layer is added between every n Bi–O bilayers in the basic compound $IPb_yBi_2Sr_2Ca_2Cu_3O_x$, a stage-n iodine-intercalated compound $I_{n+1}Pb_yBi_{2n}Sr_{2n}Ca_{2n}Cu_{3n}O_x$ is formed, with space group Bbmb and c lattice parameter $c=7+44n$ Å.

Finally, fig. 13 shows the smoothly varying interfacial structure that results at the structural transition between monolayer and bilayer intercalations. Double iodine layers collapse to single iodine layers at the positions marked by arrows, and although the

intercalation event is confined to a–b planes, there is substantial delocalized distortion of the lattice over several atomic spacings surrounding the bifurcations.

Acknowledgements

The Atomic Resolution Microscope, image analysis facilities and technical support at the National Center for Electron Microscopy are gratefully acknowledged. This research is supported by the Director, Office of Energy Research, office of Basic Energy Sciences, Materials Sciences Division, of the U.S. Department of Energy under Contract No. DeAC03-76SF00098. J.L.C. and M.L.C. are supported by National Science Foundation Grant No. DMR88-18404. J.L.C. acknowledges additional support from AT&T Bell Laboratories.

References

[1] X.-D. Xiang, S. MacKernan, W.A. Vareka, A. Zettl, J.L. Corkill, T.W. Barbee III and Marvin L. Cohen, Nature 348 (1990) 145.

[2] X.-D. Xiang, A. Zettl, W.A. Vareka, J.L. Corkill, T.W. Barbee III and Marvin L. Cohen, Phys. Rev. B 43 (1991) 11496.

[3] X.-D. Xiang, W.A. Vareka, A. Zettl, J.L. Corkill, T.W. Barbee III, Marvin L. Cohen, N. Kijima and R. Gronsky, Science 254 (1991) 1487.

[4] N. Kijima, R. Gronsky, X.-D. Xiang, W.A. Vareka, A. Zettl, J.L. Corkill and Marvin L. Cohen, Physica C 181 (1991) 18.

[5] N. Kijima, R. Gronsky, X.-D. Xiang, W.A. Vareka, A. Zettl, J.L. Corkill and Marvin L. Cohen, Physica C 184 (1991) 127.

[6] N. Kijima, R. Gronsky, X.-D. Xiang, W.A. Vareka, A. Zettl, J.L. Corkill and Marvin L. Cohen, Physica C 190 (1992) 597.

[7] N. Kijima, H. Endo, J. Tsuchiya, A. Sumiyama, M. Mizuno and Y. Oguri, Jpn. J. Appl. Phys. 28 (1989) L787.

[8] W.O. Saxton, T.J. Pitt and M. Horner, Ultramicroscopy 4 (1979) 343.

[9] R. Kilaas, in: Proc. 45th Annual Meeting of the Electron Microscopy Soc. of America, ed. G.W. Bailey (Baltimore, Md., 1987) p. 66.

[10] P.M. de Wolff, T. Janssen and A. Janner, Acta Crystallogr. A 37 (1981) 625.

[11] R. Ramesh, B. van Tendeloo, G. Thomas, S.M. Green and H.L. Luo, Appl. Phys. Lett. 53 (1988) 2220.

[12] S. Ikeda, K. Aota, T. Hatano and K. Ogawa, Jpn. J. Appl. Phys. 27 (1988) L2040.

[13] Y. Ikeda, M. Takano, Z. Hiroi, K. Oda, H. Kitaguchi, J. Takada, Y. Miura, Y. Takeda, O. Yamamoto and H. Mazaki, Jpn. J. Appl. Phys. 27 (1988) 2067.